JOURNAL OF MATERIALS SCIENCE 26 (1991) 601 - 611

Shock synthesis and synthesis-assisted shock consolidation of silicides

L. H. YU
Department of Materials and Metallurgical Engineering and Center for Explosives Technology Research, New Mexico Institute of Mining and Technology, Socorro, New Mexico 87801, USA

M. A. MEYERS
Center of Excellence for Advanced Materials, University of California, San Diego La Jolla, California 92093, USA

Shock-induced chemical synthesis and synthesis-assisted consolidation of high-temperature materials (silicides) were investigated. Niobium, molybdenum, and titanium powders mixed with silicon powders were chosen as reactant materials for shock-induced synthesis of silicides. In parallel experiments, these reactant materials were also respectively mixed with inert intermetallic compound powders of $NbSi_2$, $MoSi_2$, and Ti_5Si_3 in different proportions and were shock consolidated. Shock processing was carried out using a modification of the experimental set-up developed by Sawaoka and Akashi. The shock waves were generated in the materials by the impact of a flyer plate at a velocity of 2 km sec^{-1}. An explosive plane-wave generator was used to initiate the main explosive charge to accelerate the flyer plate. The passage of shock waves of sufficient pressure and temperature induced a highly exothermic and self-sustaining reaction between reactant materials. The shock-synthesized intermetallic compounds and the heat of reaction enhanced bonding between inert matrix materials. The proportion of reactant powder mixtures blended with inert intermetallic materials plays a very important role in the synthesis-assisted consolidation process. Characterization of compacts was done by optical microscopy, scanning electron microscopy, and X-ray diffraction. A preliminary analysis of shock-induced chemical reactions is conducted; it predicts a 30% increase in shock pressure and shock-wave velocity over those in unreacted powders. For shock synthesis, the profuse formation of voids indicates that melting of the material occurred; in contrast, unreacted regions did not exhibit porosity.

1. Introduction

Intermetallic compounds having attractive and unique properties for extended high-temperature application are being applied as structural materials [1–3]. Silicides, in particular, are intermetallic compounds suited for high-temperature applications because of their high melting point and strength retention at high temperatures. $MoSi_2$ has already been used as heating elements [4]. Shock compression processing has been applied to synthesize materials since 1961, when DeCarli and Jamieson [5, 6] synthesized diamond from rhombohedral graphite. Since then, there has been considerable research activity in materials development using this process to synthesize compounds [7–10]. This unique process can not only induce the chemical reactions between the elemental materials, but also the high pressure can produce fully dense compacts in time durations of the order of microseconds. Horie *et al.* [11, 12] have systematically investigated shock-induced chemical synthesis in intermetallic compounds. They analysed the effects of shock-wave passage in Ni–Al powder mixtures in post-shocked specimens, and classified them as follows: (a) effects of high shock-pressure and high strain rate, and (b) effects of high temperature. Once a sufficient degree of shock-induced temperature and mixing intensity are reached, highly exothermic and self-sustaining reactions can be initiated.

The concept of shock-synthesis-assisted consolidation was first applied to consolidate ceramic powders by Sawaoka and Akashi [13]. They found that the consolidation of cubic boron nitride powders by simple shock compaction alone was not sufficient to produce strong bonding between powders; therefore, they added reactant titanium, carbon, and aluminium powders to the boron nitride. The shock synthesized ceramic binder phase and heat generated were found to assist the bonding between the cubic boron nitride powders.

In this research program, three intermetallic compounds, silicides of molybdenum, titanium and niobium were chosen as inert materials to be consolidated. These intermetallic compounds are brittle and hard and are similar to ceramic materials. It is difficult

0022–2461/91 $03.00 + .12

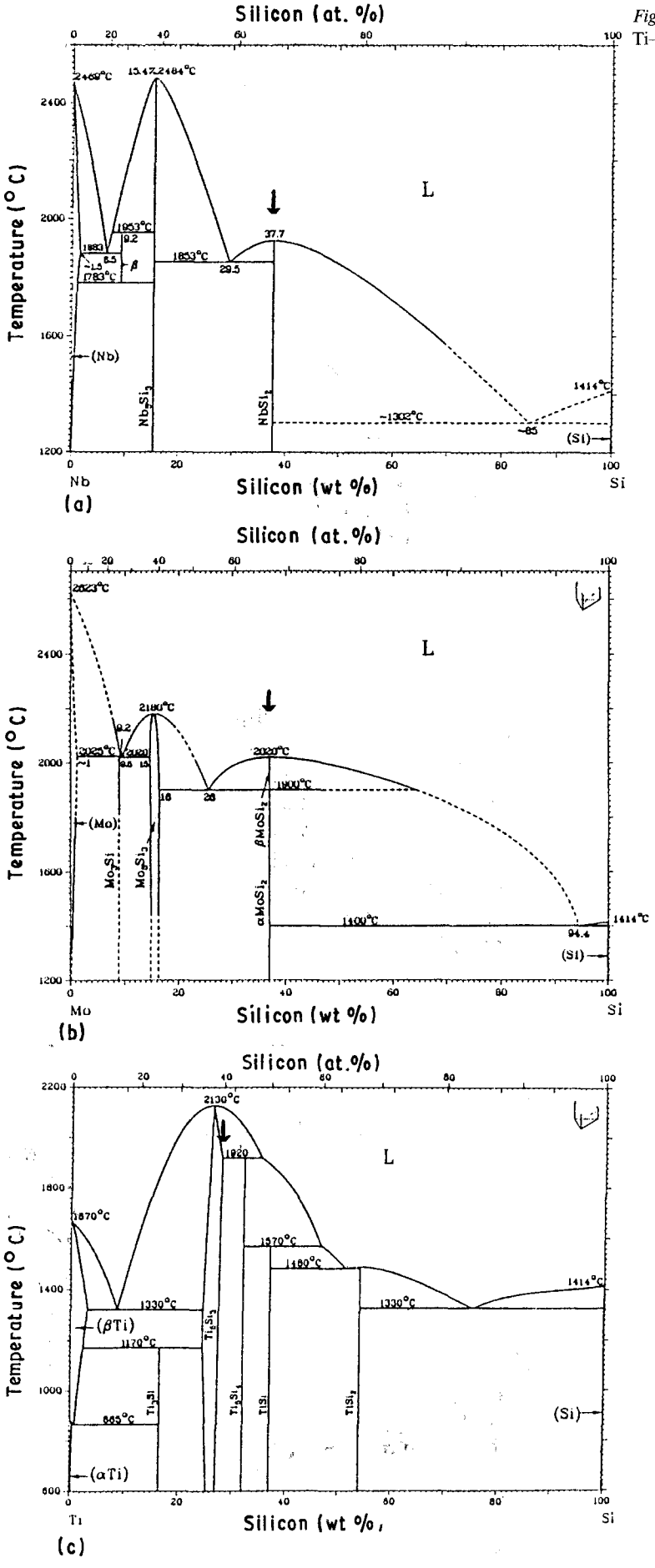

Figure 1 Phase diagrams of (a) Nb–Si, (b) Mo–Si, and (c) Ti–Si (from [14]).

to consolidate these powders by conventional techniques. The concept of shock-synthesis-assisted consolidation of ceramic powders was extended to the present work. It was demonstrated that the shock waves can induce chemical reactions between reactant materials and silicides can be synthesized to assist in the bonding between the inert intermetallic compound powders.

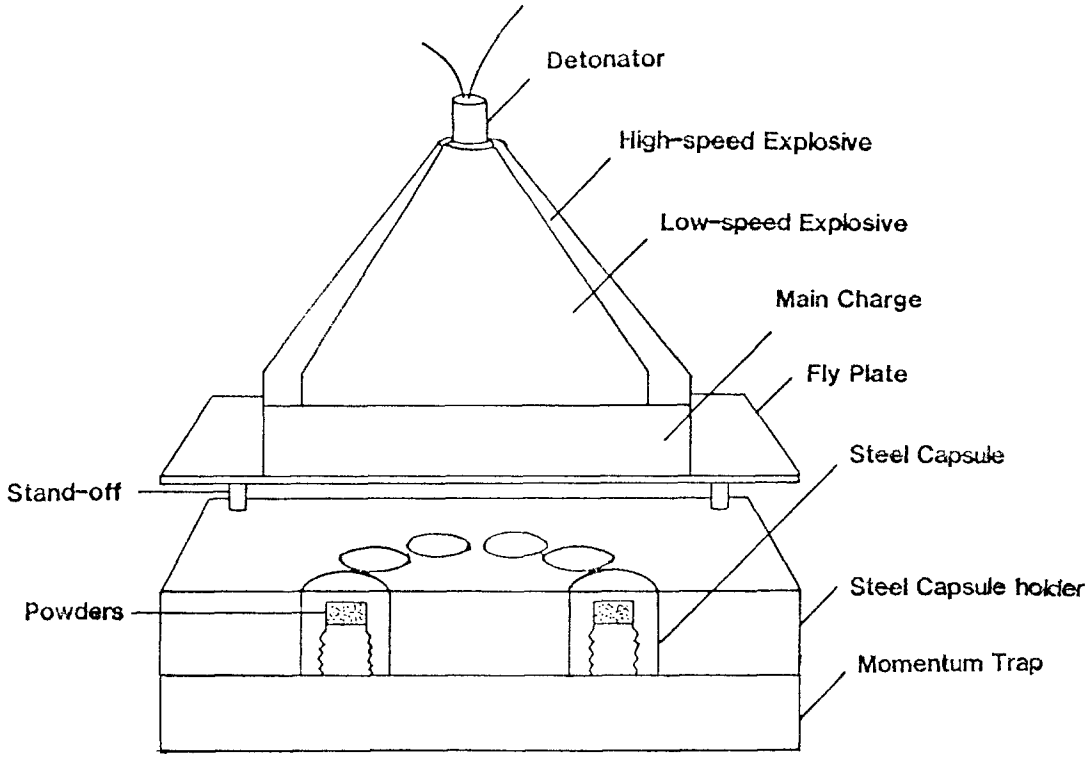

Figure 2 Section of "Sawaoka" fixture that contains twelve capsules (six shown in section).

2. Experimental procedures

Shock-induced chemical synthesis experiments were conducted on mixtures of Nb–Si, Mo–Si, and Ti–Si to determine the extent of shock induced reactions and the nature of reaction products. Shock-synthesis-assisted consolidation experiments were then conducted on powder mixtures of Nb–Si–$NbSi_2$, Mo–Si–$MoSi_2$, and Ti–Si–Ti_5Si_3. The reactant powder mixtures and intermetallics were mixed in different proportions. The powders were purchased from CERAC; their characteristics are listed in Table I. The composition of reactant materials was chosen based on the stoichiometric composition of the silicides: $NbSi_2$, $MoSi_2$, and Ti_5Si_3. Fig. 1 shows the phase diagrams of the Nb–Si, Mo–Si, and Ti–Si systems [14]. The intermetallic compounds are marked by arrows on the respective phase diagrams. The compositions of the different powder mixtures are listed in Table II. The powders were blended and loaded into the capsules in argon atmosphere.

The cross-section of the shock processing system used in the present work is schematically shown in Fig. 2. This system is an outgrowth of the earlier system used for producing high-amplitude planar shock waves. The detonation is initiated from the detonator at the top, shown in Fig. 2. A conical lens consisting of explosives with two detonation velocities was used to generate a planar wave in the main explosive charge. The flyer plate is accelerated by the detonation of the explosive charge and impacts the capsules embedded in a steel fixture. The shock waves are transmitted through the capsules into the powders. The momentum trap is used to trap the reflected tensile waves in order to recover the specimens. The

TABLE I. Powder sizes and sources.

Powder	Size (mesh)	Source	Purity (%)
Nb	− 325	CERAC	99.8
Mo	− 325	CERAC	99.9
Ti	− 325	CERAC	99.5
Si	− 325	CERAC	99.9
$NbSi_2$	− 325	CERAC	99.5
$MoSi_2$	− 325	CERAC	99.5
Ti_5Si_3	− 325	CERAC	99.5

TABLE II. Compositions of specimens and test conditions
Explosive: PBX 9404 (1.27 cm thick, 20.3 cm diameter)
Flyer plate: Steel (0.5 cm thick)
Standoff: 1 cm
Flyer plate velocity: 2 km sec^{-1}
Testing temperature: Room temperature

Sample	Powders (wt %)	Sample	Powders (wt %)
1	Nb (62) Si (38)	8	$MoSi_2$ (90) Mo (6.3) Si (3.8)
2	Mo (63) Si (37)	9	$MoSi_2$ (90) Mo (6.3) Si (3.8)
3	Ti (74) Si (26)		
4	$NbSi_2$ (90) Nb (6.2) Si (3.8)	10	$MoSi_2$ (90) Mo (6.3) Si (3.8)
5	$NbSi_2$ (70) Nb (18.6) Si (11.4)	11	$MoSi_2$ (90) Mo (6.3) Si (3.8)
6	$NbSi_2$ (50) Nb (31.0) Si (19.0)	12	$MoSi_2$ (90) Mo (6.3) Si (3.8)
7	$MoSi_2$ (90) Mo (6.3) Si (3.8)		

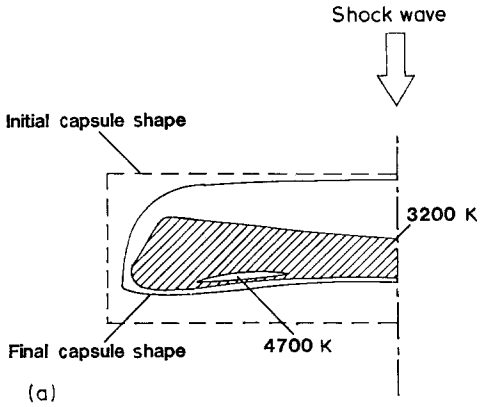

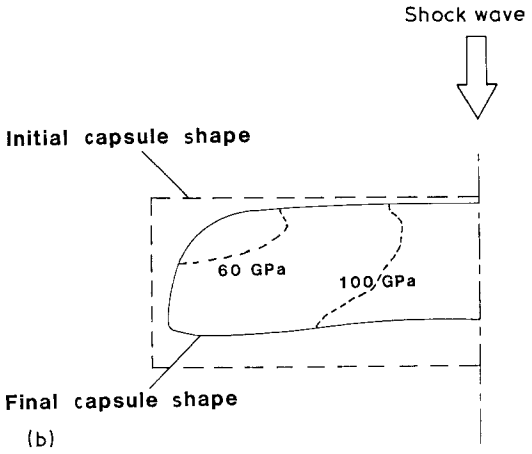

Figure 3 (a) Maximum mean bulk temperature and (b) maximum pressure profiles for Sawaoka capsule (adapted from Norwood et al. [15]).

impact velocity of flyer plate was around 2 km sec^{-1} for this experiment. The recovered specimens were characterized by optical and scanning electron microscopy and X-ray diffraction. Only the Nb–Si and Nb–Si–$NbSi_2$ systems are discussed in detail in this paper.

3. Results and discussion

The velocity of the shock wave in the powder is lower than that in the surrounding steel capsule, thus, the shock wave planarity is lost in the powder, and the lateral effects from the capsule play an important role. The pressure and temperature distributions in the powder thus become very complicated. Norwood *et al.* [15] simulated the pressure and temperature contours in powder for the Sawaoka capsules by using a two-dimensional CSQ II computer hydrocode. Fig. 3 shows the maximum pressure and mean bulk temperature contours in half cross-section of compact. These profiles can provide some information as a reference for the present experiments.

3.1. Shock synthesis of Nb–Si powders

The packing density of Nb–Si powders was 60% of the theoretical density. The morphology of niobium, silicon, and $NbSi_2$ powders is shown in Fig. 4; they have

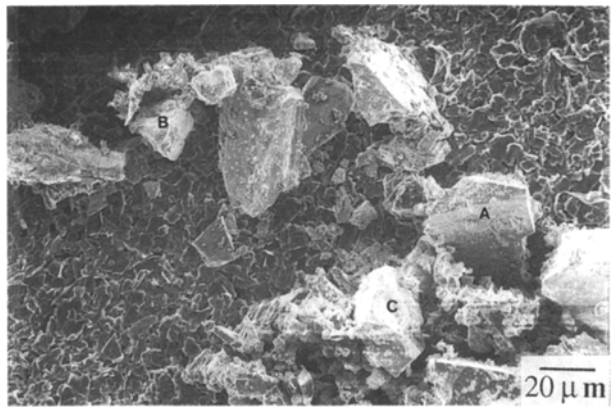

Figure 4 Size and morphology of niobium (A), silicon (B), and $NbSi_2$ (C) powders.

irregular shapes prior to compaction. The powder size, given in Table I, is below 325 mesh (~ 45 μm) for all materials. After compaction, the compacts were taken out from the capsule by machining. An optical micrograph of a part of the cross-section of the compact is shown in Fig. 5. The shock-wave propagation direction is from top to bottom. Based on the etching contrast it appears that for most of the compact the Nb–Si powders had undergone complete reaction except in the regions at the top corners. Under higher magnification, dendritic structures were found in some regions, and are shown in Fig. 6a. They are marked by arrows. Profuse voids are also found throughout the reacted regions. Fig. 6b shows the needle-like (or fibre-like) structures observed adjacent or inside voids and also proves that the voids were not produced by powder pull-out during grinding and polishing. A closer view of a void shown by scanning electron microscopy in Fig. 7 clearly delineates the inside, consisting of a maze of fibres. The synthesized phase forms as fibres, which traverse the voids. These dendrites and needles result from the shock-synthesis of compounds that involves most likely a melting and resolidification sequence.

Fig. 8 shows the morphology of the shock-synthesized regions in the Mo–Si and Ti–Si capsules, respectively. The features are analogous to the ones shown in Fig. 6: profuse voids and a homogeneous structure. EDS analysis showed no composition difference between the fibre-like structures and matrix. The profusion of voids and the microstructure emphasize that more heat was generated in this condition than for the reactionless consolidation of the powders (in the top corners). There are three possible causes for the large concentration of voids found.

(a) Shrinkage due to solidification of melted and reacted material.

(b) Tensile stresses while the synthesized material is at a high temperature and very ductile. These tensile stresses are produced by reflected waves after the passage of the main shock pulse.

(c) Expansion of the entrapped gases (or gases formed during reaction) after the passage of the shock wave.

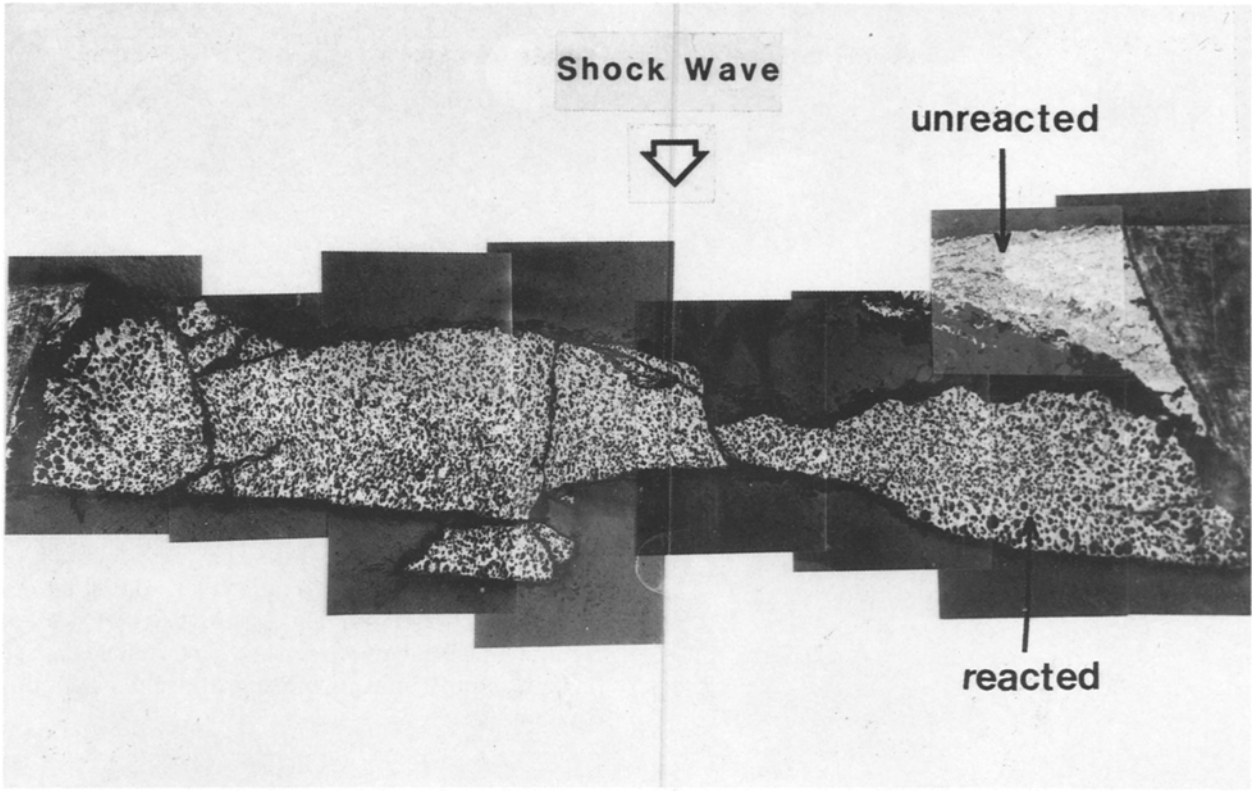

Figure 5 Optical micrograph of cross-section of Nb–Si compact. (Dark region is mounting epoxy.)

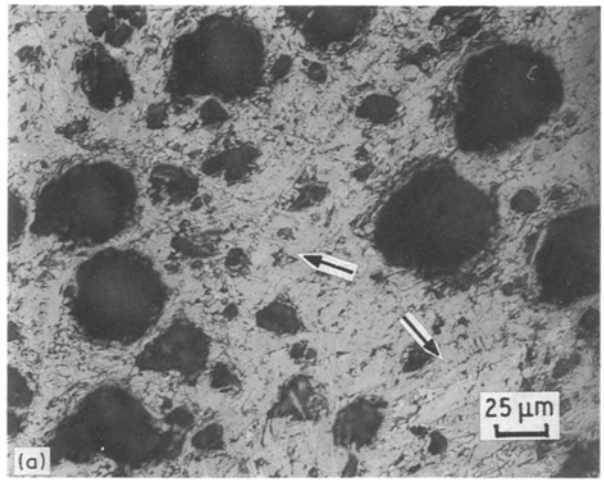

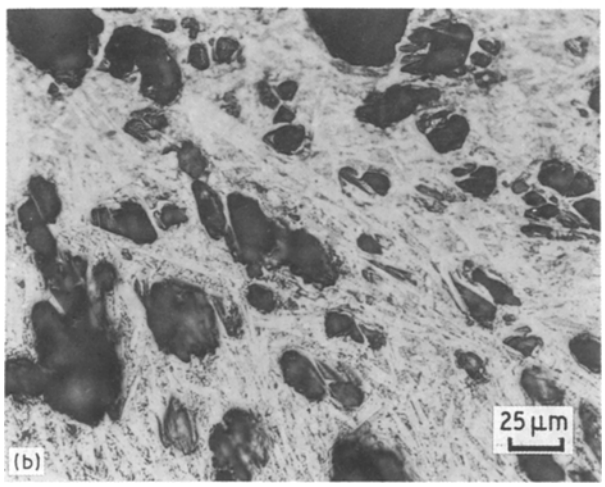

Figure 6 Optical micrographs of Nb–Si compact showing voids and (a) dendritic and (b) needle-shaped features.

In the top corners (unreacted regions), the Nb–Si powders were well compacted and interlocked together as shown in Fig. 9. Niobium and silicon powders remained unreacted probably due to lack of sufficient pressure and/or temperature to initiate the reaction in this region. The profiles shown in Fig. 3 show that the pressure and temperature in the corner regions are lower than in the other regions.

The X-ray diffraction results are shown in Fig. 10. Fig. 10a corresponds to the diffraction pattern of the starting powder mixture, and Fig. 10b corresponds to that after shock synthesis. The intermetallic compound $NbSi_2$ can be easily identified in Fig. 10b. The original niobium and silicon peaks appear to have been lost, indicating almost complete reaction.

A preliminary analysis of shock-induced chemical reactions was conducted for the present investigation. A complete analysis has been recently developed by

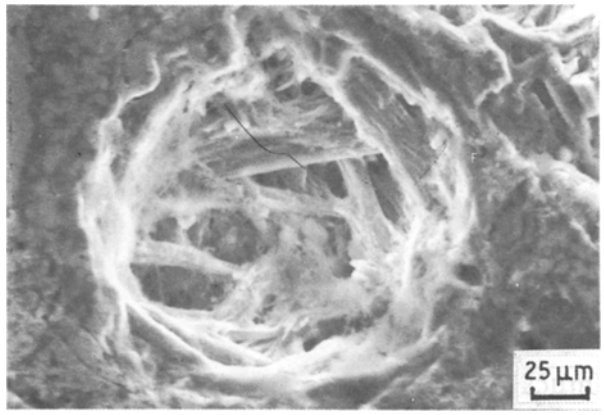

Figure 7 Scanning electron micrograph of void.

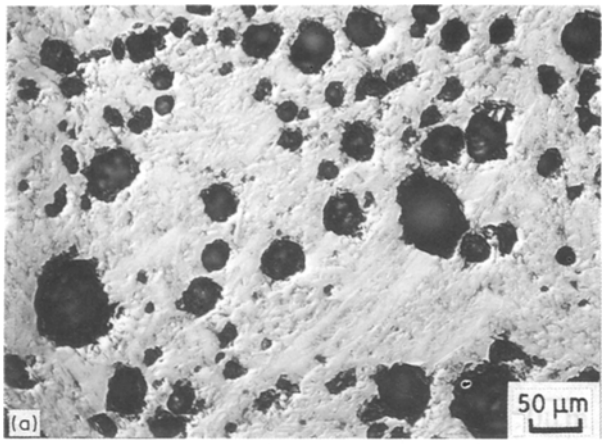

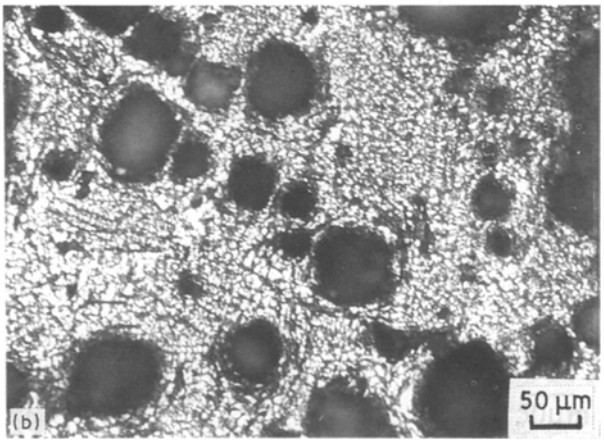

Figure 8 Optical micrographs of (a) Mo–Si and (b) Ti–Si compacts showing voids.

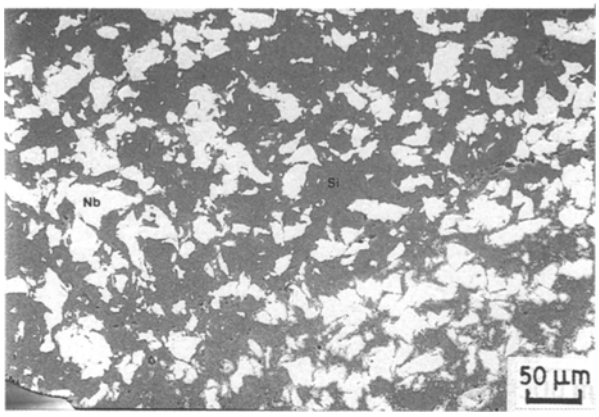

Figure 9 Micrographs of unreacted regions in Nb–Si system.

Horie and Kipp [16], but the simple analysis suffices for the purposes of this work. The basic equation of energy conservation was modified by adding an energy of reaction term. The assumptions of heat of reaction independent of pressure, zero volume change (with reaction), and no melting are implicit in this equation

$$E_2 - E_{00} = \tfrac{1}{2}P(V_{00} - V) + E_R \qquad (1)$$

where E_R is the energy of reaction at constant volume. The thermodynamic state after a complete reaction can be determined by assuming steady-state. Fig. 11 shows schematic Hugoniot pressure–volume curves for the solid material, the powder, and the powder with reaction. The curve for the reacted powder is

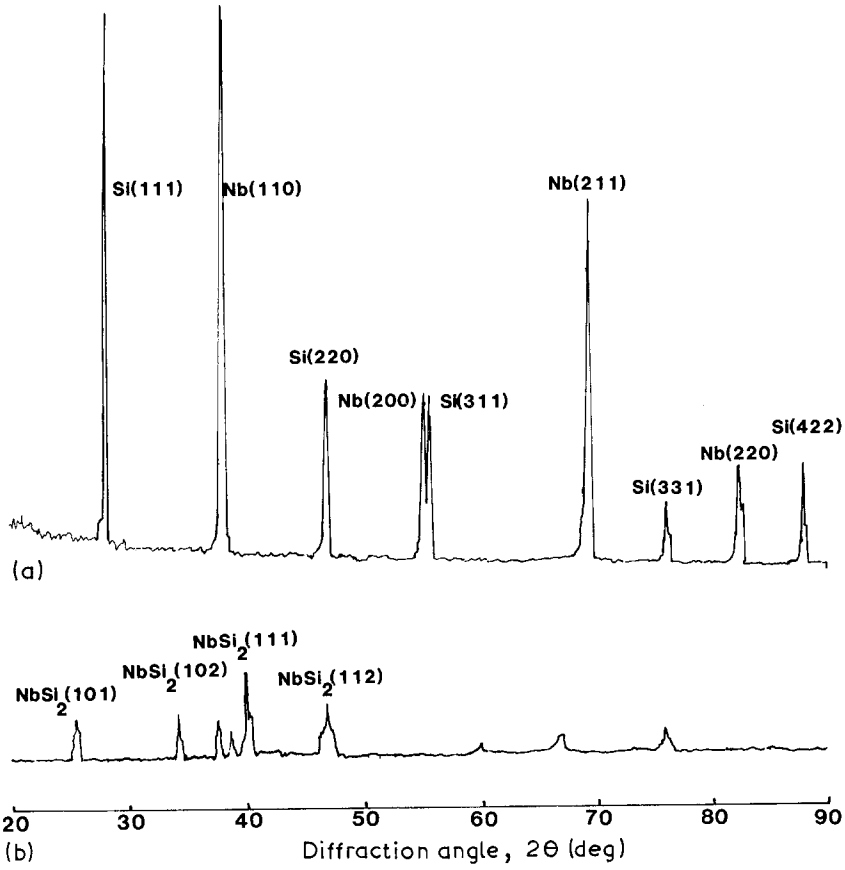

Figure 10 X-ray diffraction patterns of Nb–Si powders (a) before and (b) after synthesis and consolidation.

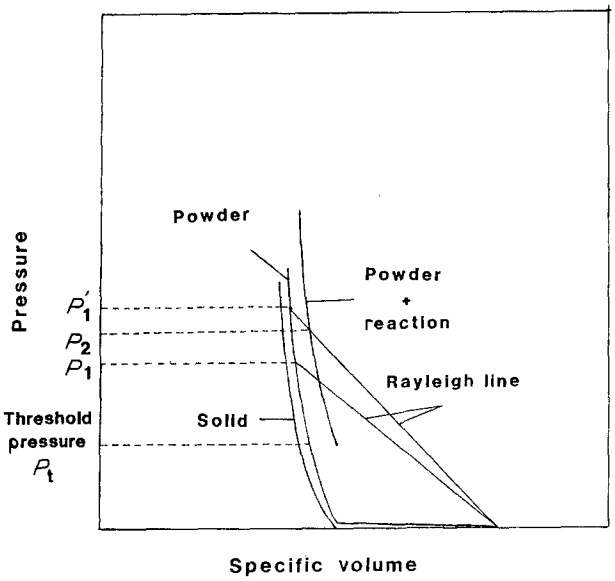

Figure 11 Schematic Hugoniots for solid, powder, and reacting powder.

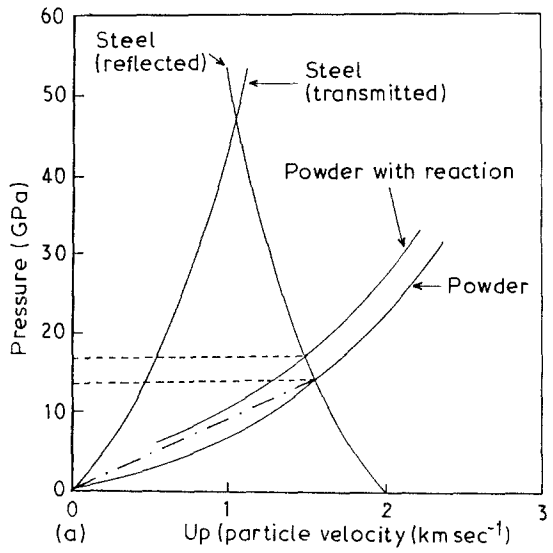

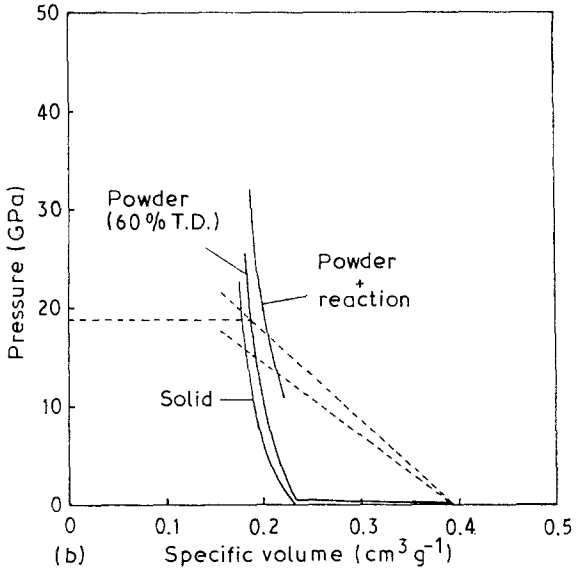

Figure 12 (a) Pressure–particle velocity curves and (b) pressure–specific volume Hugoniots for Nb(62%)–Si(38%) powders (60% TD) with and without reactions.

transposed to the right from the unreacted powder. For obtaining the Hugoniot curve for porous Nb–Si, the following procedure was adopted. The solid Hugoniot was determined by the mixing rule. First, the zero Kelvin isotherm of each component was calculated by using the Mie–Gruneisen equation of state from the solid Hugoniot. Second, the zero Kelvin isotherm of the solid mixture was determined from the zero Kelvin isotherms of the components. Third, the Hugoniot of the solid mixture was obtained from the zero Kelvin isotherm. Then, finally, the porous Hugoniot of the mixture was determined by using the Mie–Gruneisen EOS. These calculations are automatically performed in Yoshida's mixture program [17]. From the equation of state for the porous mixture, obtained from the solid mixture by Gruneisen's method (explained in detail by Altshuler [18], Meyers and Wang [19], among others), one obtains

$$P = \frac{2 - \gamma_0(V_0 - V)/V_0}{2 - \gamma_0(V_{00} - V)/V_0} P_H \qquad (2)$$

where P and P_H are the pressures for the powder and solid material at the same volume, γ_0 Gruneisen's constant, V_0 and V_{00} the specific volumes of solid and porous materials at atmospheric pressure, respectively. Using Equation 2, it is possible to calculate the internal energy for the porous material, at a volume V

$$E_1 - E_{00} = \tfrac{1}{2}P_1(V_{00} - V) \qquad (3)$$

One then uses the reactive equation (Equation 1). The energy of reaction was taken as 138 kJ mol^{-1} [20]. This value is actually for the heat of reaction, which is approximately equal to the energy for condensed systems (small PV term). The internal energy for the reacting material, at that volume, is given by

$$E_2 - E_{00} = \tfrac{1}{2}P_2(V_{00} - V) = \tfrac{1}{2}P_1(V_{00} - V) + Q \qquad (4)$$

Fig. 11 shows the three pressures P_1, P_1', and P_2. If no reaction occurs, the shock pressure is given by P_1. The additional reaction energy, E_R, released increases the pressure in the powder to P_1'. If one draws a Rayleigh line through P_1', one obtains a pressure P_2 after reaction (both shock and reaction front move at the same velocity in steady-state). One concludes that shock synthesis leads to an acceleration of reaction velocity with an increase in pressure. With the equation of state for the porous reacting material one can compute shock propagation velocities by means of Rayleigh lines. Fig. 11 also shows that P_t is required to induce reaction; if $P < P_t$, no reaction would occur.

In Fig. 12 the Hugoniot curves (pressure against particle velocity and pressure against volume) for solid, porous (60% of T.D.) and porous reacting Nb(62 wt %)–Si(38 wt %) mixture are plotted. The values used for the parameters needed in the computations are: $V_{00} = 0.38$ cm^3 g^{-1}, $V_0 = 0.23$ cm^3 g^{-1}, $\gamma_0 = 1.29$, $Q = 138$ kJ mol^{-1}. The calculations are shown for an idealized one-dimensional configuration. For a 2 km sec^{-1} flyer-plate impact velocity one obtains a shock pressure in the steel capsule of approximately 47 GPa (obtained by the impedance matching

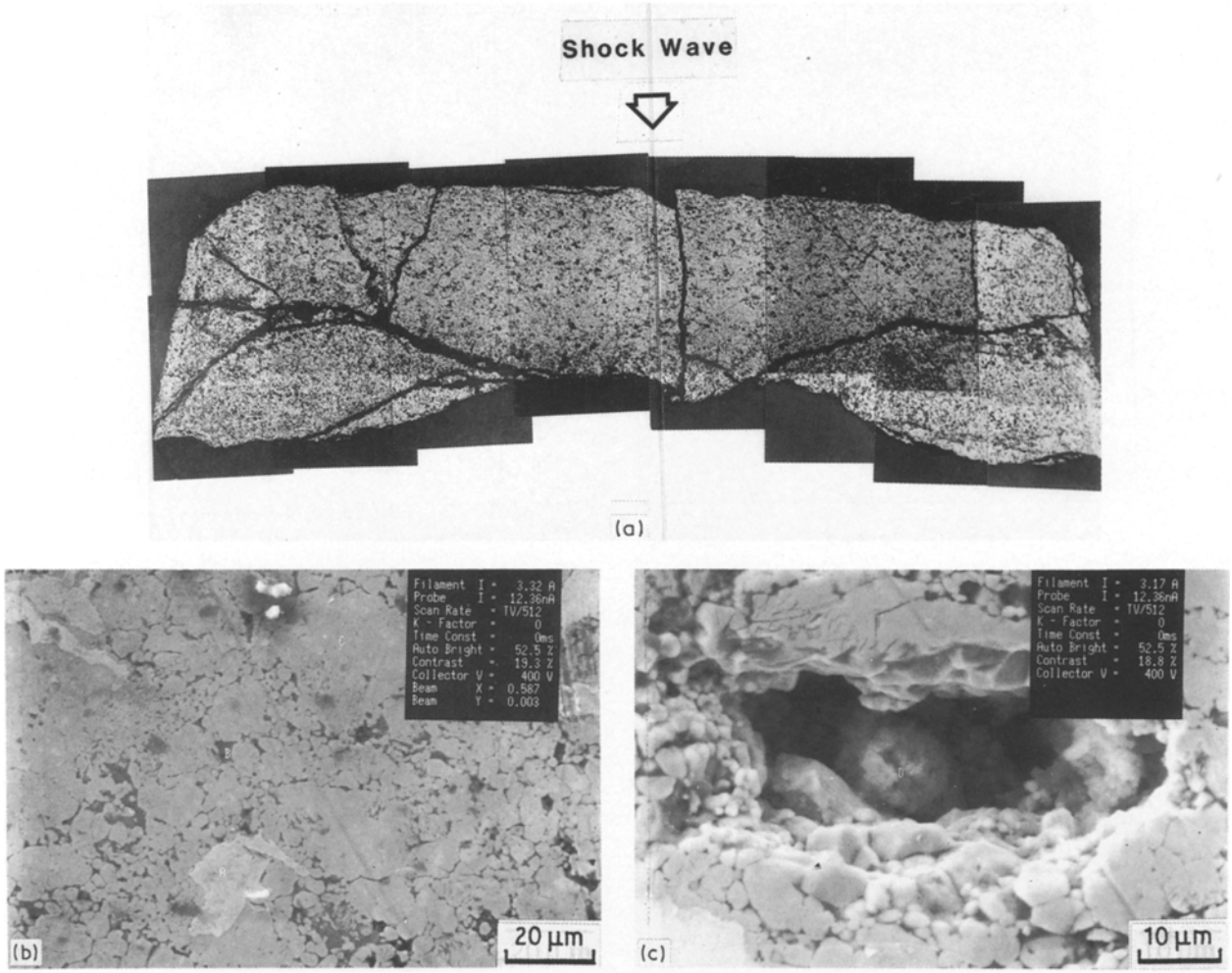

Figure 13 (a) Optical micrograph of cross-section of compact 4 (Nb 6.2 wt %, Si 19 3.84 wt %, $NbSi_2$ 90 wt %). (b) Scanning electron micrograph of local region in (a). (c) Scanning electron micrograph of void of (a).

method, shown in Fig. 12a). This will result in pressures of 14.2 and 17.2 GPa once the shock pulse enters the powder and reactive powder, respectively. These are the pressures P_1 and P_2, in Fig. 11. The pressure–volume plot of Fig. 12b is then used to obtain P'_1, the pressure in powder at the shock front (prior to reaction). Since both shock and reaction waves have the same Rayleigh slope, one finds P'_1 = 19 GPa. Thus, the reaction increases the shock pressure from 14.2 to 19 GPa, a 33% change. The increase of the shock propagation velocity is of the same order. The assumptions made in the calculations above are fairly severe and the actual changes could be significantly different.

3.2. Synthesis assisted shock consolidation

Different quantities of reactants (niobium and silicon powders) mixed in $NbSi_2$ stoichiometry were added to $NbSi_2$ powders: 10, 30 and 50 wt % for specimens 4, 5, and 6, respectively (Table II). The micrographs of the cross-sections of recovered compacts are shown in Figs 13 to 15. In Fig. 13a, the composition of the specimen was Nb–Si (10 wt %) and $NbSi_2$ (90 wt %), and most of the areas show that Nb–Si–$NbSi_2$ powders remained unreacted; however, the powders were well compacted, as shown in Fig. 13b. In this case, (in Fig. 13b) the silicon powder underwent large plastic deformation, surrounding the niobium (B) and $NbSi_2$ (A) powders, but the shock pressure and temperature were not sufficient to initiate the chemical reactions between reactant materials. The scanning electron micrograph (Fig. 13c) shows a void that does not have the same fibrous features as in the Nb–Si system. The particles are heavily deformed and have interlocked facets.

As the quantity of Nb–Si powders was increased, the extent of the chemical reaction was also observed to increase. In specimen 5 (Table II) containing 30 wt % Nb–Si powders, two different regions were observed and are shown in Fig. 14a. The top portion corresponds to the unreacted region, and the bottom portion reveals fully reacted region, in accordance with the maximum temperature profiles of Fig. 3a. Fig. 14b and 14c show a scanning electron micrograph and composition maps for silicon and niobium. It is clear that no reaction occurred; this represents the top portion of the capsule. Fig. 14c shows the reacted region. The morphology is quite different and the profuse presence of voids is noteworthy. Compositional mapping (not shown) demonstrated that reaction between niobium and silicon took place. As the quantity of the Nb–Si powders was increased to 50 wt % in specimen 6 (Fig. 15a), most areas showed

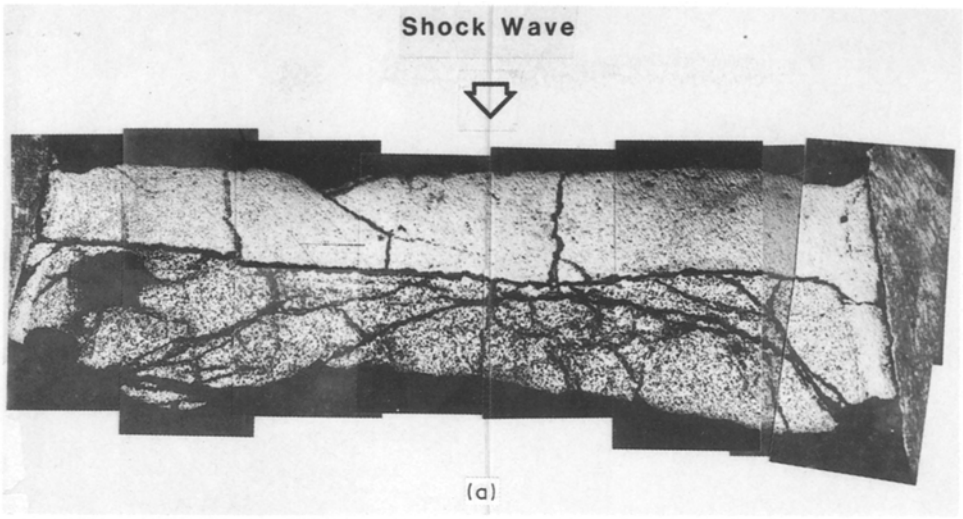

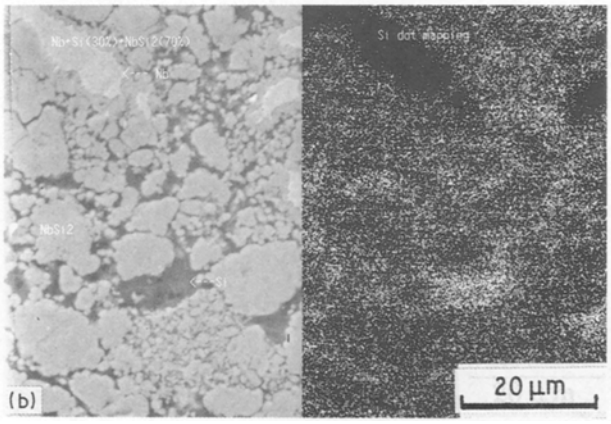

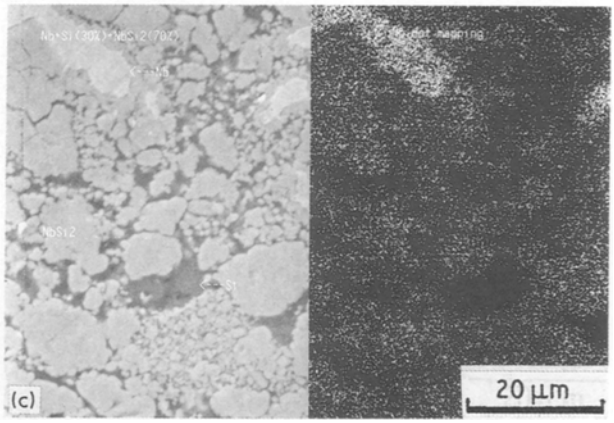

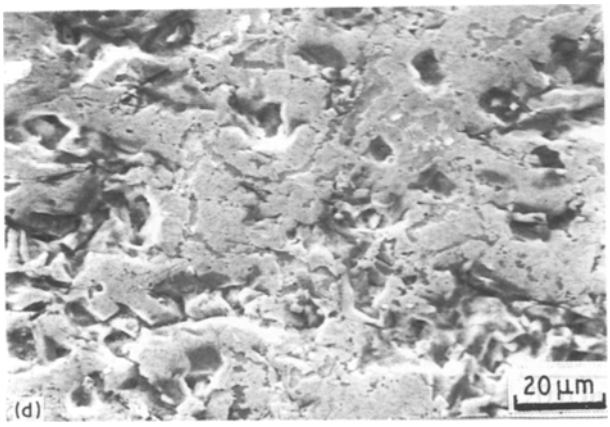

Figure 14 (a) Optical micrograph of cross-section of compact 5 (Nb 18.6 wt %, Si 11.4 wt %, $NbSi_2$ 70 wt %). (b) Scanning electron micrograph of unreacted region, silicon dot mapping. (c) Niobium dot mapping. (d) Scanning electron micrograph of reacted region.

full reaction and an appearance similar to that of specimen 1 (Nb–Si 100 wt %), shown in Fig. 5. The higher magnification micrograph of the specimen containing 50 wt % Nb–Si powder mixture is shown in Fig. 15b and 15c. The dot mapping shows that the composition is uniform. From these results, it seems that both the quantity of Nb–Si powders and shock parameters (pressure and temperature) imparted to powders have a considerable effect on the synthesis process.

The void concentrations in the reacted regions were 9% for specimen 4, 23% for specimen 5, and 30% for specimen 6, as shown in the plot in Fig. 16. The increase in the number of voids with increased proportion of reactants indicates that more shrinkage and gas evolution occurred due to the heat generated by the exothermic reaction of Nb–Si powders. X-ray diffraction patterns of three samples are shown in Fig. 17. The original niobium and silicon peaks either totally disappear or show reduced intensities for all three cases, indicating that chemical reaction is indeed induced by the passage of the shock wave. The degree of reaction depends on pressure, temperature, and the fraction of reactant materials.

4. Conclusions

It has been demonstrated that niobium, molybdenum, and titanium silicides can be synthesized by shock compression. The detailed analysis of the Nb–Si and Nb–Si–$NbSi_2$ systems showed that the reacted regions have a large fraction of porosity that can be due to several reasons. The extent of reaction decreases with the increased fraction of intermetallic compound powders added to the mixture. A preliminary calculation was conducted that shows that shock-induced reaction may cause an increase in shock pressure and velocity.

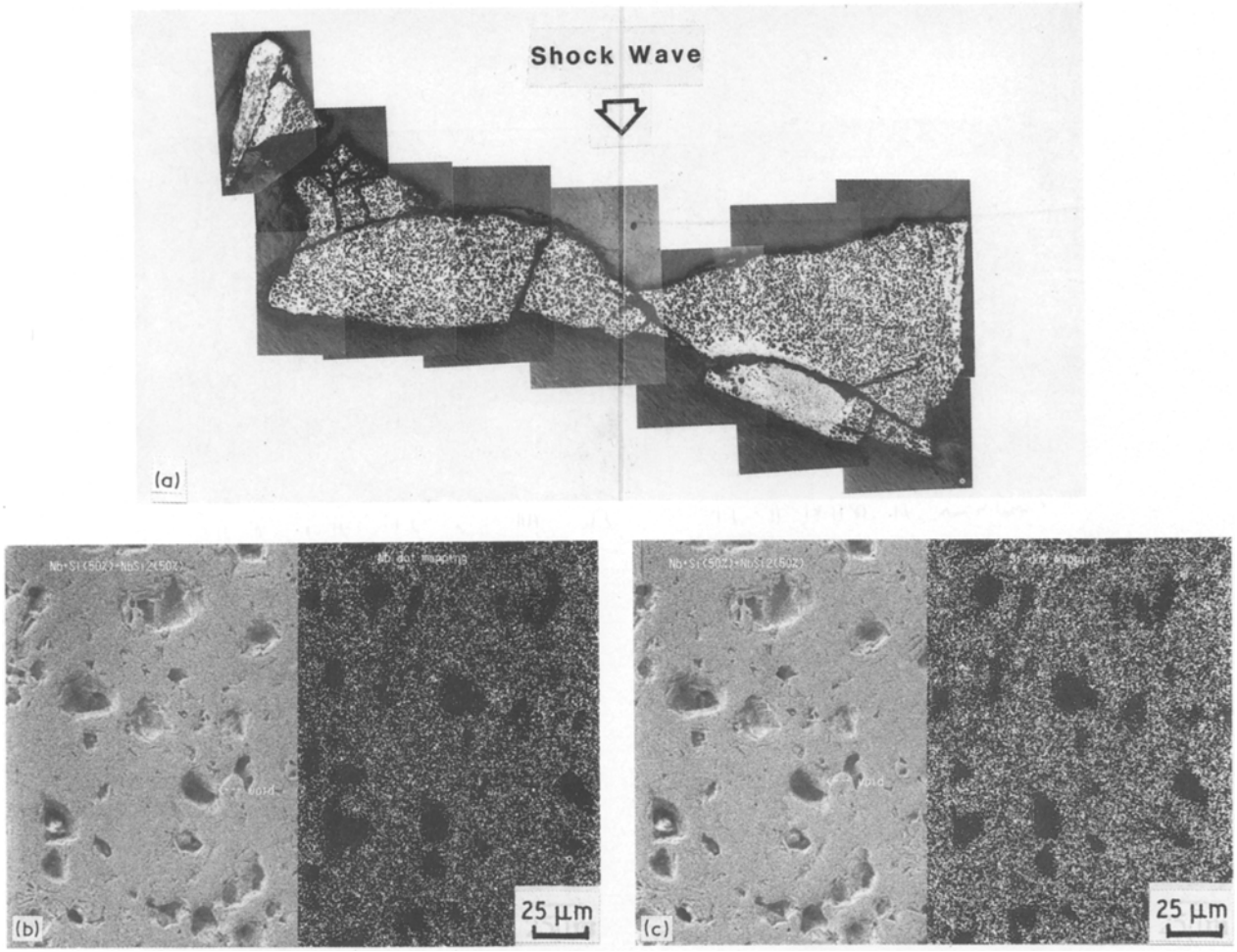

Figure 15 (a) Optical micrograph of cross-section of compact 6 (Nb 31 wt %, Si 19 wt %, $NbSi_2$ 50 wt %). (b) Scanning electron micrograph with silicon dot mapping. (c) Scanning electron micrograph with niobium dot mapping.

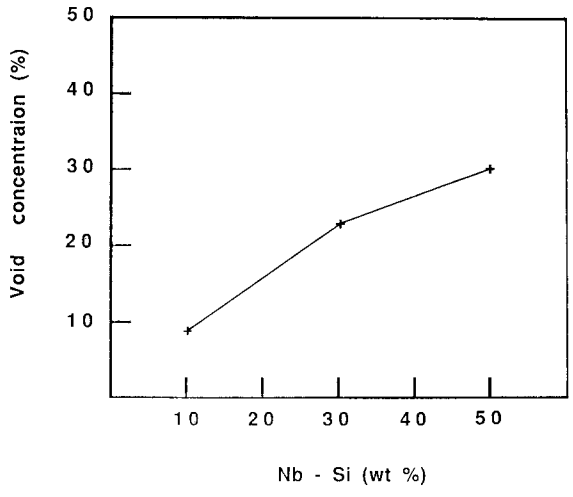

Figure 16 Void concentration plotted against Nb–Si weight percentage.

Acknowledgements

This research was sponsored by McDonnell Douglas Research Laboratories and by the National Science Foundation Materials Processing Initiative (latter stages). The support provided by Dr C. Whitsett and P. Meschter is gratefully acknowledged. The capable help of Mr T. Gould in setting up the experiments is greatly appreciated. The electron microscopy was conducted at the University of California, San Diego through the auspices of the Center of Excellence for Advanced Materials. Discussions with Dr W. Nellis (LLNL), who suggested the use of the P-U_p plot for pressure determination in case of reaction, and with J. M. Lee (New Mexico Tech) are gratefully appreciated. Dr N. N. Thadhani (New Mexico Tech) was helpful in all stages of this investigation and carefully reviewed the manuscript; his contribution was very valuable.

References

1. J. H. WESTBROOK, *Metall. Trans.* **8A** (1977) 1327.
2. H. A. LIPSITT, D. SHECHTMAN, and R. E. SCHAFRIK, *ibid.* **6A** (1975) 1991.
3. D. SHECHTMAN, M. J. BLACKBURN and H. A. LIPSITT, *ibid.* **5A** (1974) 1373.
4. Z. A. MUNIR, *Ceram. Bull.* **67** (1988) 342.
5. P. S. DeCARLI, US Patent 3 238 019 March, (1966).
6. P. S. DeCARLI and J. C. JAMIESON, **133** (1961) 821.
7. S. S. BATSANOV, A. A. DERIBAS, E. V. DULEPOV, M. G. ERMAKOV and V. M. KUDINOV, *Comb. Expl. Shock Waves USSR* **1** (1965) 47.
8. A. N. DREMIN and O. N. BREUSOV, *Russ. Chem. Rev.* **37** (1968) 392.
9. R. A. GRAHAM, B. MOROSIN, E. L. VENTURINI and M. J. CARR, *Ann. Rev. Mater. Sci.* **16** (1986) 315.
10. Y. KIMURA, *Jpn. J. Appl. Phys.* **2** (1963) 312.

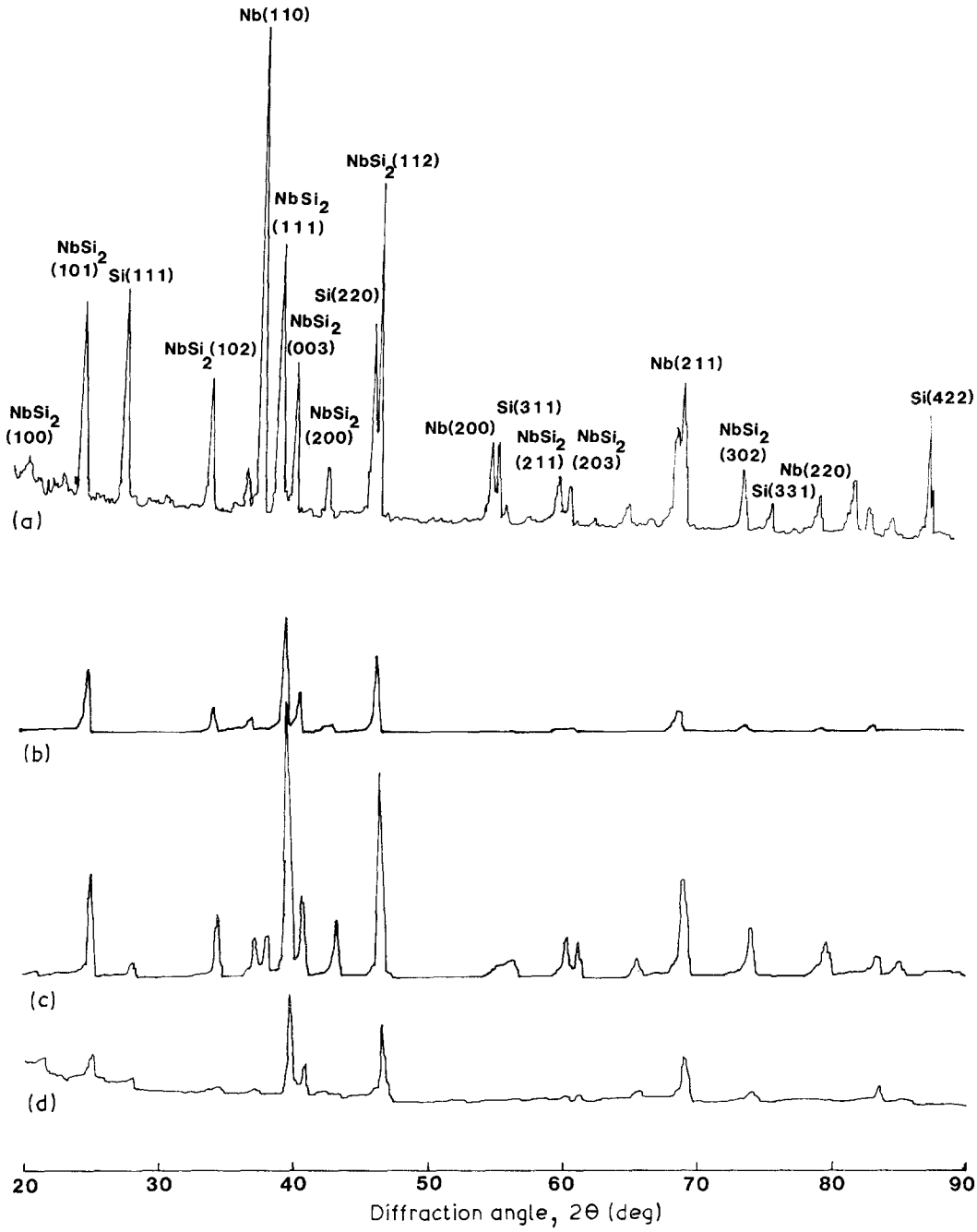

Figure 17 X-ray diffraction patterns of Nb–Si–$NbSi_2$ powders (a) before (Nb 31 wt %, Si 19 wt %, $NbSi_2$ 50 wt %) and (b) (Nb 6.2 wt %, Si 3.8 wt %, $NbSi_2$ 90 wt %), (c) (Nb 18.6 wt %, Si 11.4 wt %, $NbSi_2$ 70 wt %) and (d) (Nb 31 wt %, Si 19 wt %, $NbSi_2$ 50 wt %) after synthesis and consolidation.

11. Y. HORIE, R. A. GRAHAM and I. K. SIMONSEN, *Mater. Lett.* **3** (1985) 354.
12. I. K. SIMONSEN, Y. HORIE, R. A. GRAHAM and M. J. CARR, *ibid.* **5** (1987) 75.
13. A. B. SAWAOKA and T. AKASHI, US Patent 4655830 (1987).
14. T. B. MASSALSKI "Binary Alloy Phase Diagrams" (American Society for Metals, Metals Park, Ohio, 1986).
15. F. R. NORWOOD, R. A. GRAHAM and A. SAWAOKA, in "Shock Waves in Condensed Matter", edited by Y. M. Gupta (Plenum, New York, 1986) p. 837.
16. Y. HORIE and M. J. KIPP, *J. Appl. Phys.* **63** (1988) 5718.
17. M. YOSHIDA, Mixture Program, Report, Center for Explosives Technology Research, New Mexico Institute of Mining and Technology, Socorro, New Mexico, 1986.
18. L. V. ALTSHULER, *Sov. Phys.* **8** (1965) 52.
19. M. A. MEYERS and S. L. WANG, *Acta Metall.* **36** (1988) 925.
20. O. KUBASCHEWSKI and C. B. ALCOCK, "Metallurgical Thermochemistry" (Pergamon, New York, 1979).

Received 26 July 1989
and accepted 19 February 1990